buildings

MDPI

Article

Elastic Local Buckling and Width-to-Thickness Limits of I-Beams Incorporating Flange–Web Interactions

Lei Zhang [1], Qianjing Zhang [1], Genshu Tong [1,*] and Qunhong Zhu [2]

[1] Institute of Advanced Engineering Structures, Zhejiang University, Hangzhou 310058, China; celzhang@zju.edu.cn (L.Z.); 11612047@zju.edu.cn (Q.Z.)
[2] Institute of Engineering Cost, Zhejiang College of Construction, Hangzhou 311215, China
* Correspondence: tonggs@zju.edu.cn

Abstract: The local buckling of I-section beams is investigated with the flange–web interactions taken into account. Using numerical results employing the finite element method and a semi-analytical method, the flange–web interactions of I-sections and their effects on the buckling stresses are explored and discussed. Simple approximate solutions for the buckling coefficients of the web and compressive flange are developed using the energy method, and they are refined using the numerical results. Using the simple solutions for buckling coefficients, the limits for the width-to-thickness ratio of the compressive flange and web of I-section beams are then proposed. Comparisons with the results of existing solutions and provisions in design codes imply that the proposed solutions are superior in predicting the limits for width-to-thickness ratios, and they are capable of accounting for the flange–web interactions at the local buckling of I-section beams.

Keywords: local buckling; I-section; flange–web interaction; bending; width-to-thickness ratio

check for updates

Citation: Zhang, L.; Zhang, Q.; Tong, G.; Zhu, Q. Elastic Local Buckling and Width-to-Thickness Limits of I-Beams Incorporating Flange–Web Interactions. *Buildings* **2024**, *14*, 347. https://doi.org/10.3390/buildings14020347

Academic Editor: Francesco Ascione

Received: 25 December 2023
Revised: 23 January 2024
Accepted: 24 January 2024
Published: 26 January 2024

1. Introduction

The strength of thin-walled members is frequently governed by local buckling failure. To prevent the premature local buckling, the width-to-thickness ratios of the plate elements of thin-walled sections are limited in design codes (e.g., GB50017 [1], AISC360 [2], and EC3 [3]). In current design codes, each plate element of a thin-walled section is nearly treated as an isolated plate in determining its width-to-thickness limit, and its boundary conditions are normally assumed to be simply supported, clamped, or partially restrained. However, existing studies have revealed that plate elements may strongly interact at areas of local buckling via the intersections in between, and these interactions may have significant effects on the local buckling strengths.

Although the local buckling of thin-walled sections has attracted much attention over recent decades [4–20], investigations accounting for the interactions between the plate elements are relatively few and have been conducted mainly through numerical methods. The local buckling behaviors of thin-walled sections subjected to axial compression, major axis bending, and minor axis bending were investigated by Seif and Schafer [9] using the finite strip method. In their study, the non-dimensional parameter $\eta = (h/t_{\mathrm{w}})(2t_{\mathrm{f}}/b_{\mathrm{f}})$ (where b_{f} and t_{f} are the width and thickness of the flange, respectively, and h and t_{w} are the height and thickness of the web, respectively,) was proposed to consider the plate element interactions, and simple solutions for the buckling coefficients that were dependent on the unique parameter η were then developed. Using the finite strip method, Gardner et al. [10] presented the following solution for the local buckling stresses of thin-walled sections:

$$\sigma_{\mathrm{cr,cs}} = \sigma_{\mathrm{cr,p}}^{\mathrm{SS}} + \zeta\left(\sigma_{\mathrm{cr,p}}^{\mathrm{F}} - \sigma_{\mathrm{cr,p}}^{\mathrm{SS}}\right), \tag{1}$$

where $\sigma^{SS}_{cr,p} = \min\left(\sigma^{SS}_{cr,f}, \sigma^{SS}_{cr,w}\right)$, $\sigma^{F}_{cr,p} = \min\left(\sigma^{F}_{cr,f}, \sigma^{F}_{cr,w}\right)$, the subscripts "f" and "w" respectively stand for the flange and web, and the superscripts "SS" and "F" represent the simply supported and fixed conditions of the plate element, respectively. In this solution, the buckling stress of a plate element ($\sigma_{cr,cs}$) is gained by interpolating between the buckling stresses of the plate element with simply supported ($\sigma^{SS}_{cr,p}$) and fixed conditions ($\sigma^{F}_{cr,p}$), and the coefficient ζ, used to consider the interactions between adjacent plate elements, is a function of the parameter $\phi = \sigma^{SS}_{cr,f}/\sigma^{SS}_{cr,w}$. Gardner et al. [10] found that ϕ is essentially identical to the parameter η as presented by Seif and Schafer [9]. Simple solutions were also given by Gardner et al. [10], where the interactions between the buckling coefficients of the flange and web of the I-sections were relevant to t_f/t_w and ϕ. It should be noted that in their solutions, the same expression for the interactive parameter ζ was used for the interpolation between $\sigma^{SS}_{cr,p}$ and $\sigma^{F}_{cr,p}$ for the sections subjected to different loads, indicating that the interaction behaviors between the plate elements were independent of the stress distributions in the cross-section.

A similar interpolation method (Equation (2)) was adopted by Jin et al. [11] in which the interaction coefficient ζ was given as follows:

$$\zeta = \frac{3\kappa}{3\kappa + 1}, \tag{2}$$

where κ is the ratio of the free torsional rigidities of the flange and web (i.e., $\kappa = b_f t_f^3 / h t_w^3$). It is worth mentioning that the use of the interaction coefficient ζ implies that the flange provides a rotational restraint equal to the free torsional rigidity of the web at the flange–web conjunction, which may be overestimated for I-sections under axial compression in many cases (where h/b is not greater than 10 [15]). Based on the general beam theory, a parametric study was conducted by Vieira et al. [12] through numerical analyses, where the rectangular hollow sections with equally thick flanges and webs were subjected to a combined axial force, and biaxial bending was considered. Expressions for the buckling stress that were capable of considering the stress distribution variations in the cross-sections were given. The values of the constants for these expressions were listed in a table, and they mainly depended on the aspects of the cross-sections. An inelastic analysis method was developed by Ragheb et al. [13] in which I-sections, regardless of the stress distributions, were divided into a series of strips in the uniformly distributed axial stresses. By taking into account the residual stress and initial deflection, the width-to-thickness limits for the I-sections under axial compression and bending were presented.

As mentioned above, most of the existing studies on the local buckling of thin-walled sections have been based on numerical analyses where the interactions between the plate elements are considered. Moreover, there has been a lack of simple solutions for buckling stresses and the width-to-thickness limits for thin-walled sections incorporating the interactions between plate elements of the thin-walled sections. Based on a previous study on I-section columns [15], this paper presents a systematical study on the local buckling of I-section beams, with flange–web interactions taken into account. Approximate solutions for the buckling stresses are presented based on the energy method, and they were validated using the results of the finite element analysis and a semi-analytical solution. Using the parameter η, as presented by Seif and Schafer [9], simple solutions are then proposed for the buckling coefficients, which were in very good agreement with the FE results. New limits for the width-to-thickness ratios of I-sections under pure bending are also presented, and they are capable of precisely considering the flange–web interactions at the local buckling. Comparisons with the FE results and predictions of existing solutions and design codes imply the very good performance of the proposed solutions.

2. Finite Element Analysis

2.1. Finite Element Modeling

Finite element (FE) analyses were performed using the general FE software ANSYS 17.0. The FE modeling used herein was similar to that in [15] for I-columns, except for the different loading conditions. As shown in Figure 1, the I-section beam was modeled using the SHELL63 elements of ANSYS. SHELL63 is a four-node, thin-shell element with six degrees of freedom at each node, and it is suitable for large deformation analyses [21]. To simulate the simply supported boundary conditions at both ends, the translations in the z and y directions of both beam ends were restrained (Figure 1). The displacement along the x-direction of the middle height of the web was also restrained to eliminate the rigid body motion. The bending moments were applied at both beam ends via a series of nodal forces along the longitudinal direction. At each node, the nodal force was calculated by considering the width and thickness of the element, in addition to the stress distributions due to the pure bending, being uniform in the flanges and linear variations in the web.

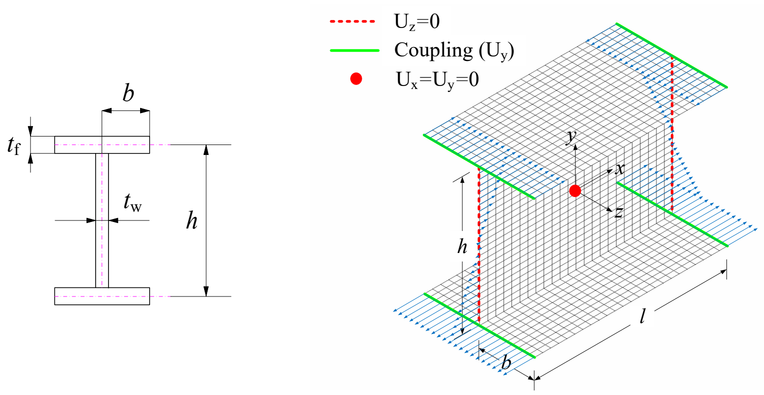

Figure 1. I-section subjected to pure bending (FE model).

The local buckling behaviors of I-sections under pure bending were investigated using eigenvalue buckling analyses on a total of 329 I-sections. For the FE analyses, b = 200 mm and t_f = 10 mm were adopted for all I-sections (see Figure 1), while the values of h/b and t_f/t_w varied from 1.0 to 10.0 and 0.7 to 4, respectively. A much wider range of h/b ratios was adopted in this study for the I-beams compared to that used in reference [15] for I-sections subjected to the axial compression, which was due to the consideration that I-sections with large h/b ratios are frequently utilized in flexural members for achieving good bending–resisting capacities.

A critical local buckling stress might be defined at the local minimum, the point of inflection, or the distinct transition between the local and global buckling on the signature curve [10]. In this study, the local minimum was used for all the specimens, as the latter two cases usually exist in L- and T-sections under combined axial compression and bending [10]. In gaining the buckling stress of the local minimum, for each I-section, a series of FE analyses were performed, with the length l varying from 0.3h to 5.0h, and then the minimal buckling stress σ_{crb} and the corresponding length a could be obtained.

2.2. Results and Discussions

As long as the critical local buckling stress is known, the buckling coefficient can be back-calculated using Equation (3), as follows:

$$k_{wb} = \sigma_{crb} \frac{12(1-\mu^2)h^2}{\pi^2 E t_w^2}, \quad (3)$$

where E and μ are, respectively, the elastic modulus and Poisson's ratio of the material and h and t_w are the height and the thickness of the web, respectively (Figure 1). It is noteworthy that the cross-section in the FE modeling was represented with the mid-surface line for all the plates.

The relationships between $K_{wb,\,FE,}$ and the non-dimensional parameter η ($\eta = \frac{h}{b}\frac{t_f}{t_w}$) for I-beams with different ζ ratios ($\zeta = \frac{t_f}{t_w}$) are depicted in Figure 2a, where K_{wb} and $_{FE}$ are the buckling coefficients of the web, and they were calculated using the buckling stresses σ_{crb} from the FE analysis and considering the relationship in Equation (3). It can be seen from Figure 2a that the use of the non-dimensional parameter η from Seif and Schafer [9] was beneficial for achieving a good correlation between the buckling coefficients of the I-sections, accounting for the flange–web interactions. As is shown in Figure 2a, K_{wb} and $_{\mathrm{FE}}$ increased with η due to the increments in the rotational restraint of the flange to the web. After the ascending branch, K_{wb} and $_{\mathrm{FE}}$ reached a plateau, indicating that the restraint of the flange was close to that of the fixed condition. The relationships between K_{wf} and $_{\mathrm{FE}}$, the buckling coefficient of the compressive flange, and the parameter η are plotted in Figure 2b. The relationship $K_{\mathrm{fb,FE}} = K_{\mathrm{wb,FE}}/\eta^2$ was adopted for obtaining the values of K_{wf} and $_{\mathrm{FE}}$, as the compressive stress in the flange was equal to the maximal compressive stress in the web when the cross-section was subjected to major axis bending.

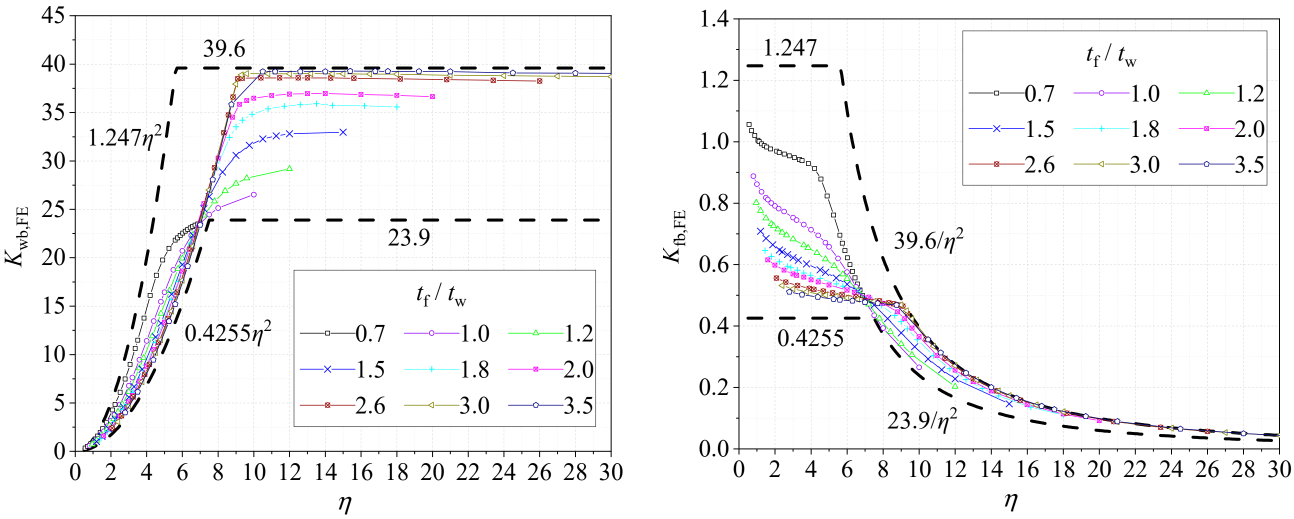

(**a**) K_{wb} (**b**) K_{fb}

Figure 2. FE results of local buckling coefficients for the I-sections under pure bending.

Gardner et al. [10] found that the relationship $\min\left(\sigma_{\mathrm{cr,f}}^{\mathrm{SS}}, \sigma_{\mathrm{cr,w}}^{\mathrm{SS}}\right) \leq \sigma_{\mathrm{cr,cs}} \leq \min\left(\sigma_{\mathrm{cr,f}}^{\mathrm{F}}, \sigma_{\mathrm{cr,w}}^{\mathrm{F}}\right)$ was always satisfied for I-sections subjected to pure bending, where $\sigma_{\mathrm{cr,cs}}$ stands for the minimal buckling stress of the cross-section and the other variables represent the minimal buckling stresses of the isolated plates under simply supported (with the superscript "SS") and fixed boundary conditions (with the superscript "F"). The subscripts "f" and "w" represent the flange and web, respectively. The above-mentioned relationship could be converted into $\min\left(0.4255\eta^2, 23.9\right) \leq K_{\mathrm{wb}} \leq \min\left(1.247\eta^2, 39.6\right)$ and $\min\left(0.4255, 23.9/\eta^2\right) \leq K_{\mathrm{fb}} \leq \min\left(1.247, 39.6/\eta^2\right)$ by considering the buckling stresses of the isolated plates. Consequently, the upper and lower bounds of K_{wb} and K_{fb} could be obtained, as illustrated in Figure 2a,b with the black dashed lines.

2.3. Comparison with Analytical Solutions

For the elastic local buckling of I-sections under axial compression, a theoretical solution has been presented, and buckling stresses can be obtained by solving a differential equation and considering the boundary conditions [15]. Very good agreement has been found between the analytical and FE results. However, this theoretical solution is not applicable to loading conditions other than axial compression. An analytical approach was also presented in the study by Ragheb [22] on the elastic local buckling of pultruded FRP sections under eccentric compression. In his approach, the web, with the stress gradient, was divided into strips under axial compression (Figure 3). A differential equation could be created for each strip, and they were treated as thin plates under the axial compression. By applying the continuity conditions between adjacent strips and the boundary conditions, the characteristic transcendental equation in matrix form could be obtained. By assuming the buckling displacements, the buckling stresses could be solved via a numerical program.

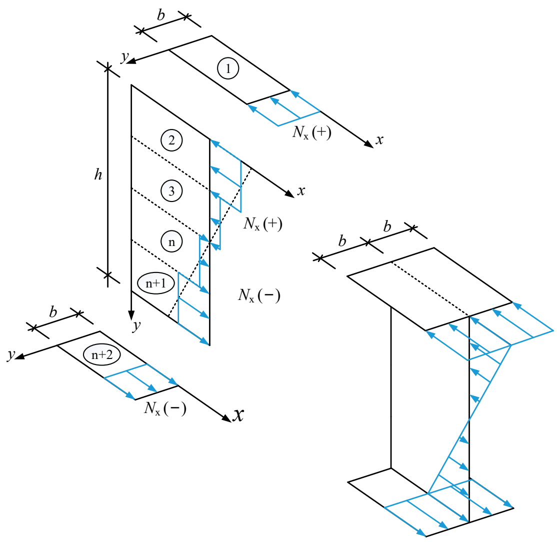

Figure 3. Modeling of a steel I-shaped section subjected to pure bending.

The analytical approach presented by Ragheb [22] was modified in this study to solve the buckling stress of the I-section beams under pure bending. In doing so, each of the flanges was divided to two strips of the same dimensions, while n = 10 was adopted for the web division. Following the method established by Ragheb [22], a matrix ($4n$ + 8 and $4n$ + 8) for the characteristic transcendental equation was obtained. A Matlab code was then developed for solving the characteristic transcendental equation, with which the buckling coefficients, $K_{\mathrm{wb,t}}$ and $K_{\mathrm{wf,t}}$, could be calculated (Figure 4). As shown in Figure 4a,b, the buckling coefficients from the FE analyses and analytical approach matched very well, indicating that both methods were reliable.

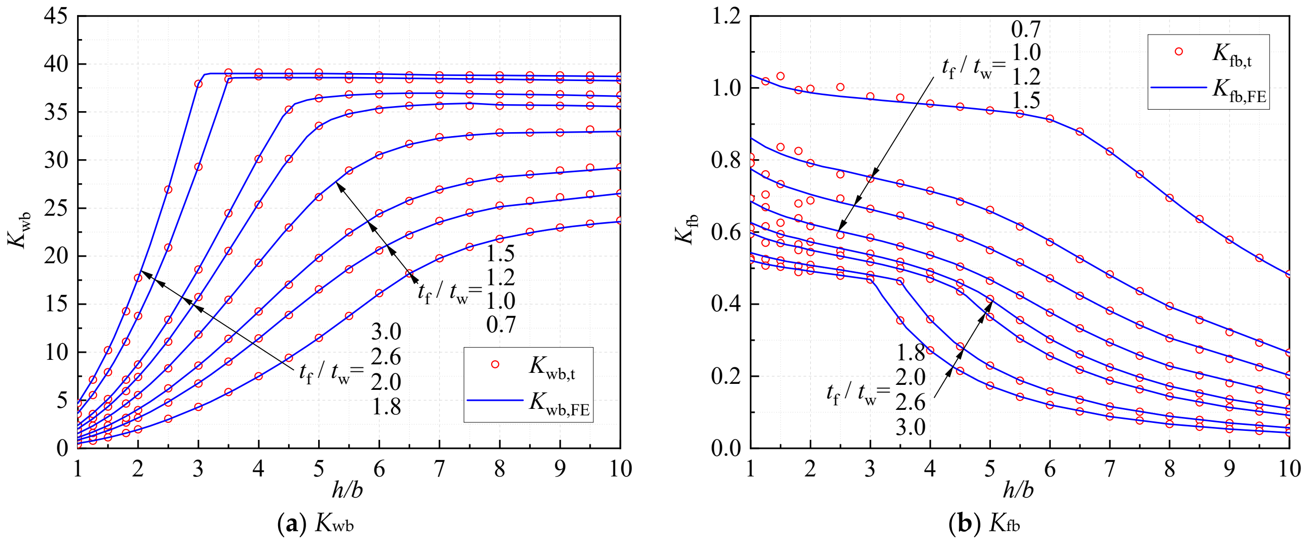

Figure 4. Comparisons of the local buckling coefficients with the theoretical results.

2.4. Buckling Mode

The flange–web interactions at the local buckling could be seen in the buckling modes given in Table 1. For each value of t_f/t_w, three typical I-sections were chosen to show the flange-dominated, weak-interaction, and web-dominated buckling modes. In the middle column of Table 1, the weak-interaction buckling modes correspond to the cases where $\sigma^{\mathrm{SS}}_{\mathrm{cr,f}} = \sigma^{\mathrm{SS}}_{\mathrm{cr,w}}$. It can be seen from Table 1 that strong interactions between the web and compressive flange may have occurred, while the tensile flanges were nearly in their original configurations, in most cases, which meant that it was reasonable to assume the tensile flange as the fixed boundary of the web.

Table 1. Typical buckling modes from the FE analysis.

Case	Flange-Dominated Mode	Weak Interaction	Web-Dominated Mode
$t_f/t_w = 0.7$	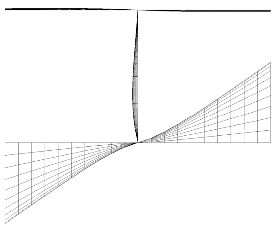	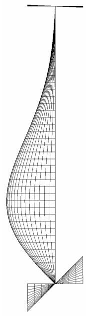	
	$h/b = 1$	$h/b = 10$	
$t_f/t_w = 1.2$	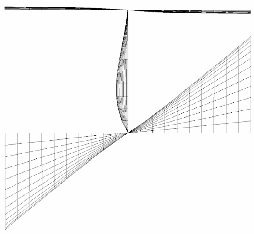	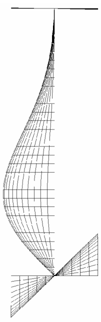	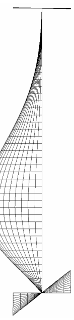
	$h/b = 1$	$h/b = 6.2$	$h/b = 10$
$t_f/t_w = 1.8$	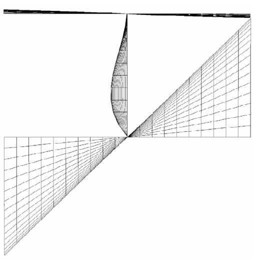	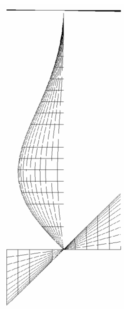	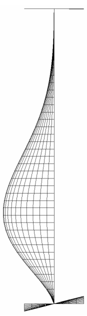
	$h/b = 1$	$h/b = 4.2$	$h/b = 10$
$t_f/t_w = 2.6$	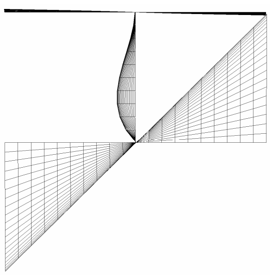	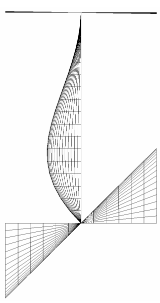	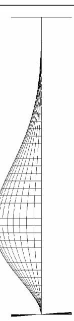
	$h/b = 1$	$h/b = 2.8$	$h/b = 10$

3. Simple Solution Development

3.1. Energy Method

Approximate solutions for the elastic local buckling coefficients of the I-beams were derived through the energy method, which was further used in the development of the width-to-thickness ratio limits of the compressive flange and web.

The total potential of a thin plate under uniaxial compression is given by the following [5]:

$$\prod = \frac{1}{2}D\iint\left\{\left(\frac{\partial^2 w}{\partial x^2}+\frac{\partial^2 w}{\partial y^2}\right)^2 - 2(1-\mu)\left[\frac{\partial^2 w}{\partial x^2}\frac{\partial^2 w}{\partial y^2} - \left(\frac{\partial^2 w}{\partial x \partial y}\right)^2\right]\right\}\mathrm{d}x\mathrm{d}y - \frac{1}{2}\iint\left(N_{\mathrm{x}}\left(\frac{\partial w}{\partial x}\right)^2\right)\mathrm{d}x\mathrm{d}y, \quad (4)$$

where x and y are the coordinates along the longitudinal and transverse directions, respectively, w is the deflection of the plate, N_{x} is the axial load per unit of width, t is the thickness of the plate, and D is the flexural rigidity of the plate per unit of width ($D = Et^3/12(1-\mu^2)$, where E is the elastic modulus and μ is the Poisson's ratio of the material).

Two local Cartesian coordinate systems, x-1-y_1 and x-2-y_2, were established for the compressive flange and web, respectively (Figure 5).

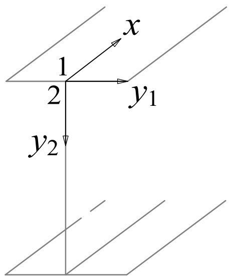

Figure 5. Local coordinate systems.

For the I-sections during bending, the axial load per unit of width in the compressive flange (N_{xf}) and web (N_{xw}) were given by the following:

$$N_{\mathrm{xf}} = \sigma t_{\mathrm{f}} \text{ and} \quad (5)$$

$$N_{\mathrm{xw}} = \sigma\left(1 - 2\frac{y_2}{h}\right)t_{\mathrm{w}}, \quad (6)$$

where σ is the longitudinal stress at the mid-face of the compressive flange and the maximum compressive stress of the web. The deflection of the web was assumed to be as follows:

$$w_{\mathrm{w}}(x, y_2) = A\left(\sin\frac{\pi y_2}{h} + \frac{\sqrt{634}}{100}\sin\frac{2\pi y_2}{h} + \frac{1}{75}\sin\frac{3\pi y_2}{h}\right)\sin\frac{\pi x}{a}, \quad (7)$$

where a is the half-length of the buckling mode in the longitudinal direction.

It should be noted that the deflection function of Equation (7) satisfied all boundary conditions. As illustrated in Equation (7), three terms were adopted in this deflection function, where the constants were determined based on the buckling mode corresponding to the minimal buckling load of the simply supported plates, with a large a/h ratio. For detailed information on the development of this equation, readers are referred to [23]. By substituting Equations (6) and (7) into Equation (4), the total potential of the web could be derived as follows:

$$\prod_{\mathrm{w}} = \frac{D_{\mathrm{w}}}{4}ah\left(\frac{634}{625}\frac{\pi^4}{h^4} + \frac{47{,}861}{90{,}000}\frac{\pi^4}{a^4} + \frac{1569}{1250}\frac{\pi^4}{a^2h^2}\right)A^2 - \frac{\sigma t_{\mathrm{w}}}{4}ah\frac{5072\sqrt{634}}{140{,}625}\frac{\pi^2}{a^2}A^2. \quad (8)$$

The deflection of the compressive flange was assumed to be as follows:

$$w_{\mathrm{f}}(x, y_1) = C\frac{y_1}{b}\sin\frac{\pi x}{a}. \tag{9}$$

At the flange–web conjunction, $\left.\frac{\partial w_{\mathrm{w}}}{\partial y_2}\right|_{y_2=0} = \left.\frac{\partial w_{\mathrm{f}}}{\partial y_1}\right|_{y_1=0}$ needed to be satisfied due to the rotational continuity at the flange–web conjunction, which provided the following:

$$C = 1.5436\frac{\pi b}{h}A. \tag{10}$$

Using Equation (10), Equation (9) could also be written as follows:

$$w_{\mathrm{f}}(x, y_1) = 1.5436\frac{\pi y_1}{h}A\sin\frac{\pi x}{a}. \tag{11}$$

Substituting Equations (5) and (11) into Equation (4), the total potential of the compressive flange could be obtained as follows:

$$\prod\nolimits_{\mathrm{f}} = 2(1.5436)^2 A^2\frac{\pi^2 b^2}{h^2}\frac{1}{b^2}\left\{\frac{\pi^4 b D_{\mathrm{f}}}{12a}\left[\frac{b^2}{a^2} + \frac{6(1-\nu)}{\pi^2}\right] - \frac{\sigma t_{\mathrm{f}}\pi^2 b^3}{12a}\right\}. \tag{12}$$

Taking $\frac{\partial(\prod_{\mathrm{f}} + \prod_{\mathrm{w}})}{\partial A}$ to be zero provided the following:

$$\begin{gathered}\left[2.3827\frac{2\pi^2}{3}\frac{t_{\mathrm{f}}b^3}{h} + h^2 t_{\mathrm{w}}\frac{5072\sqrt{634}}{140{,}625\pi^2}\right]\sigma = \\ \frac{\pi^2 E}{12(1-\nu^2)}\left\{2.3827\frac{2\pi^2}{3}\frac{b}{h}\left[\frac{b^2}{a^2} + \frac{6(1-\nu)}{\pi^2}\right]t_{\mathrm{f}}^3 + \left(\frac{634}{625}\frac{a^2}{h^2} + \frac{47{,}861}{90{,}000}\frac{h^2}{a^2} + \frac{1569}{1250}\right)t_{\mathrm{w}}^3\right\}\end{gathered}. \tag{13}$$

Applying $\frac{\partial\sigma}{\partial a} = 0$ to Equation (13) provided the following:

$$\alpha_{\min} = \frac{a}{h} = \sqrt[4]{15.455\frac{b^3 t_{\mathrm{f}}^3}{h^3 t_{\mathrm{w}}^3} + 0.5242}, \tag{14}$$

where $\alpha_{\min}$ is the normalized half-length of buckling mode corresponding to the minimal local buckling stress σ_{cr}. Substituting Equation (14) into Equation (13) provided the following:

$$\sigma_{cr} = \frac{\pi^2 E t_{\mathrm{w}}^2}{12(1-\mu)h^2}\frac{2\sqrt{0.54 + 15.90\frac{\zeta^6}{\eta^3}} + 6.67\frac{\zeta^4}{\eta} + 1.26}{15.68\frac{\zeta^4}{\eta^3} + 0.09}, \tag{15}$$

where $\zeta = \frac{t_{\mathrm{f}}}{t_{\mathrm{w}}}$ and $\eta = \frac{h t_{\mathrm{f}}}{b t_{\mathrm{w}}}$.

Then, the buckling coefficient could be obtained as follows:

$$K_{\mathrm{wb1}} = \frac{2\sqrt{0.54 + 15.90\frac{\zeta^6}{\eta^3}} + 6.67\frac{\zeta^4}{\eta} + 1.26}{15.68\frac{\zeta^4}{\eta^3} + 0.09}. \tag{16}$$

As is shown in Figure 6, the buckling coefficients derived from the energy method (K_{wb1}) were in good agreement with the FE results ($K_{\mathrm{wb,FE}}$) for $\zeta > 1.5$ and relatively small h/b values. However, the comparisons in Figure 6 show that K_{wb1} was always greater than $K_{\mathrm{wb,FE}}$ for greater h/b values, and it may have exceeded the upper limit of K_{wb}. Therefore, based on the FE results, the maximum values for K_{wb1} could be derived from Equation (17). The predictions from Equation (17) (K_{wbm}) were compared with those from the FE analyses ($K_{\mathrm{wbm,FE}}$), and as shown in Figure 7, they matched well.

$$K_{\mathrm{wbm}} = 29.8 + 9.5\tanh[1.35(\zeta - 1.3)]. \tag{17}$$

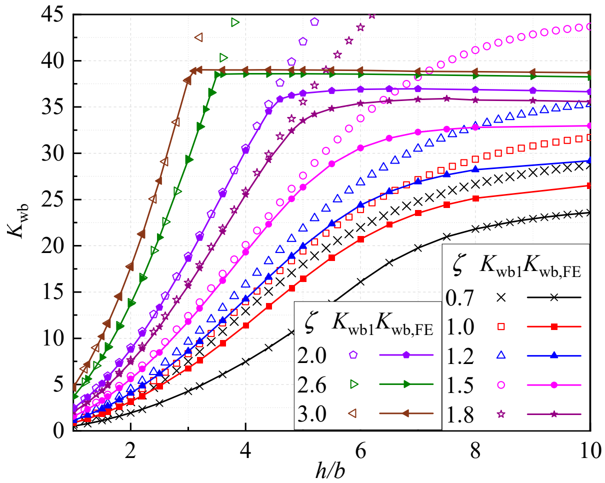

Figure 6. Comparison of the buckling coefficients.

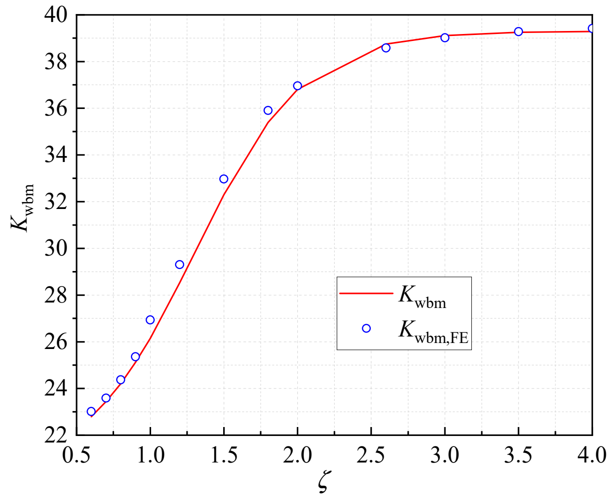

Figure 7. Comparison of the maximum values of K_w (Equation (17)) with the FE results.

Besides the maximum values, significant differences between K_{wb1} and $K_{wb,FE}$ could be seen in many cases, as shown in Figure 6, especially for the I-sections with small values for ζ (i.e., $\zeta < 1.5$). This was mainly due to the discrepancies between the assumed and actual buckling modes (see Figure 8), which may have resulted in the overestimation in the buckling load in employing the energy method. We compared the buckling modes with the FE results, and as seen in Figure 8, the assumed buckling modes in Equations (7) and (9) are shown using red solid lines.

The expression of K_{wb1} was further modified, and the new solution for the buckling coefficient of the web could then be given as follows:

$$K_{wbs} = \tanh(1.2\zeta)\rho K_{wb1} < K_{wbm} \text{ and} \tag{18}$$

$$\rho = \begin{cases} 0.02\left(\frac{h}{b} - 3\right)^2 + 0.85 < 1.9 - \zeta & \text{for } \zeta < 1.0 \\ \rho = 1.0 & \text{for } \zeta \geq 1.0, \end{cases} \tag{19}$$

where K_{wb1} and K_{wbm} are as given in Equations (16) and (17), respectively.

Comparisons between the predictions of Equation (18) and the FE results were made, and as shown in Figure 9 ($\zeta < 1.0$) and Figure 10 ($\zeta \geq 1.0$), good matches were found. As shown in Figure 9b, the buckling coefficients of the compressive flange could be calculated using $K_{fbs} = K_{wbs}/\eta^2$. It is worth mentioning that $\zeta\left(= t_f/t_w\right) < 1.0$ was not practical for the I-sections under pure bending, although it was covered in this study.

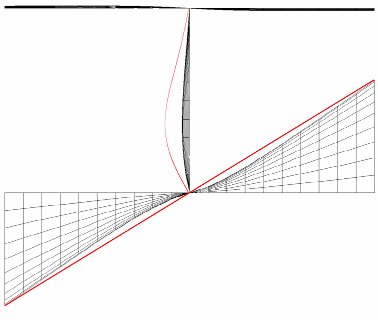

(a) t_f/t_w=0.7, h/b=1.0

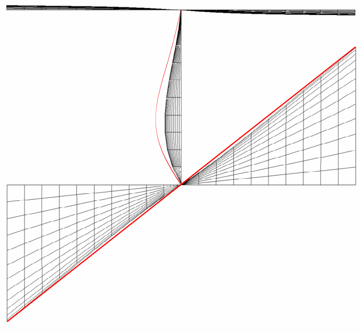

(b) t_f/t_w=1.2, h/b=1.0

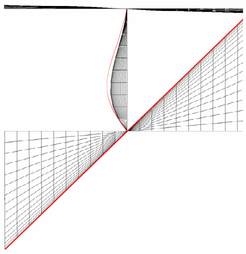

(c) t_f/t_w=1.8, h/b=1.0

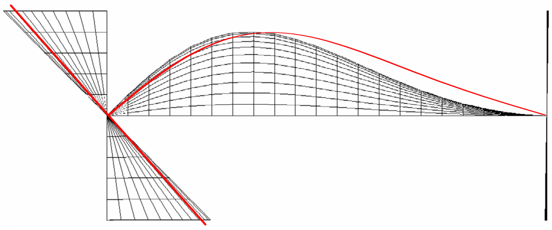

(d) t_f/t_w=1.8, h/b=4.2

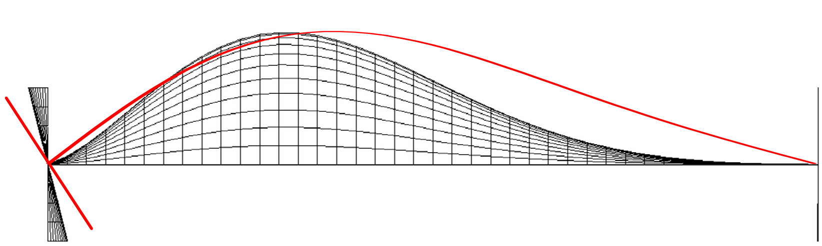

(e) t_f/t_w=1.8, h/b=10.0

Figure 8. Comparison of the buckling modes.

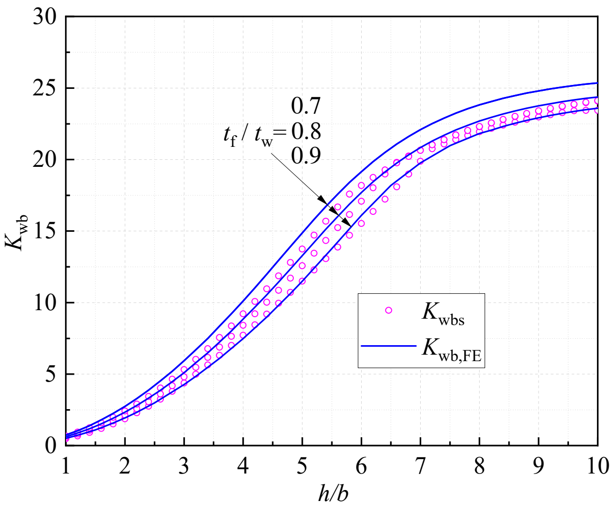

(**a**) K_{wb}

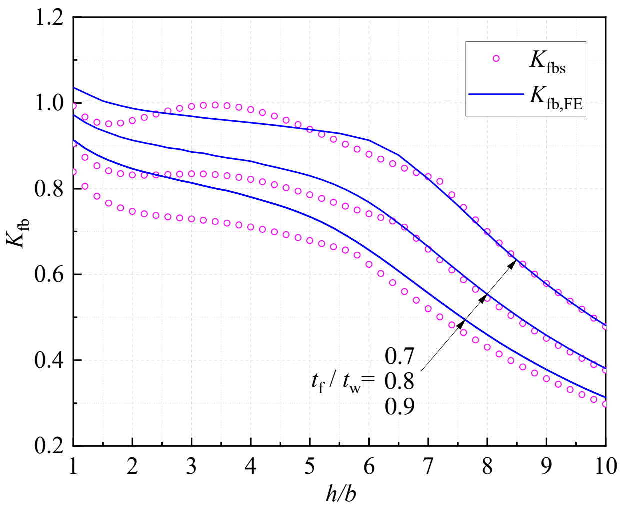

(**b**) K_{fb}

Figure 9. Comparisons of the modified buckling coefficients with the FE results (t_f/t_w < 1).

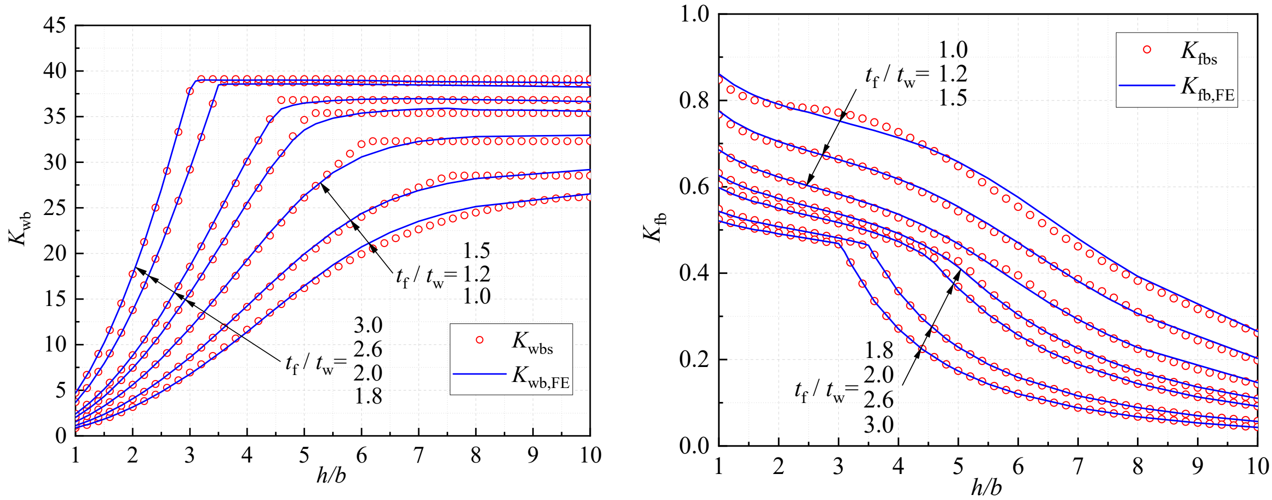

(**a**) K_{wb} (**b**) K_{fb}

Figure 10. Comparisons of the modified buckling coefficients with the FE results ($t_f/t_w \geq 1$).

3.2. Comparison with Existing Solutions

A simple expression of the web buckling coefficient of I-sections under major axis bending (Equation (20)) was developed by Seif and Schafer [9] through the finite strip analyses using CUFSM, as follows:

$$k_w = \frac{1}{1.5/\eta^2 + 0.015}. \tag{20}$$

The buckling coefficient k_w illustrated in Equation (20) is related to a single variable, η, which is different from the solution illustrated in Equation (18), depending on the values of both η and ζ. The buckling coefficients of the compressive flange and the web from Equation (18) were compared with those from the solution established by Seif and Schafer [9] and the FE analyses shown in Figure 11. It can be seen from Figure 11 that the simple solution established Seif and Schafer [9] may provide conservative predictions in most cases.

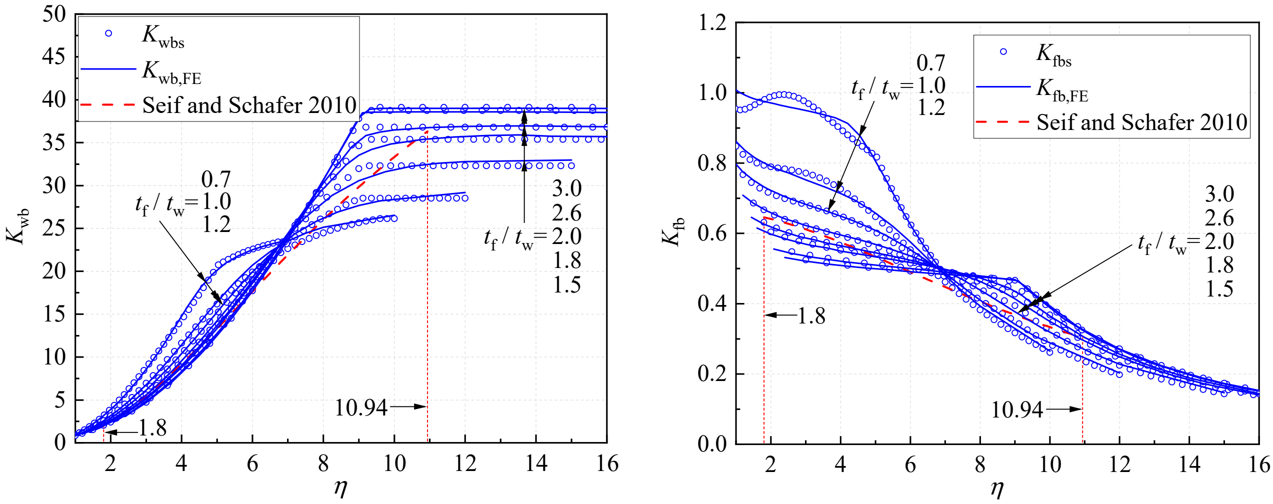

(**a**) K_{wb} (**b**) K_{fb}

Figure 11. Comparison of the buckling coefficients with existing solutions [9].

Employing the same software (CUFSM v4.03), the local buckling of the structural steel sections under different loading conditions were studied by Gardner et al. [10]. In their study, the web of an I-section was regarded as a thin plate with boundary conditions between the simply supported and fixed conditions due to the flange–web interaction at the site of the local buckling. The formulas for the buckling coefficients were then developed. For the case studied in this paper (i.e., I-sections subjected to pure bending), the buckling coefficients of the web can be expressed as follows:

$$K_{\mathrm{wb,G}} = \begin{cases} \eta^2(0.4255 + 0.8215\psi_{\mathrm{f}}) & \eta < 5.64 \\ 0.4255(1-\psi_{\mathrm{f}})\eta^2 + 39.6\psi_{\mathrm{f}} & 5.64 \le \eta < 7.49, \\ 23.9 + 15.7\psi_{\mathrm{w}} & \eta \ge 7.49 \end{cases} \tag{21}$$

where ψ_{f} and ψ_{w} are the parameters accounting for restraining the flanges, and they can be obtained as follows:

$$\psi_{\mathrm{f}} = 0.00267\zeta\eta^2 \ge \frac{0.4 - 0.00445\eta^2}{\zeta} \text{ and} \tag{22}$$

$$\psi_{\mathrm{w}} = \zeta\left(0.45 - \frac{946.5}{\eta^4}\right). \tag{23}$$

As shown in Figure 12a,b, the predictions of Equation (18) were compared with those of Equation (21) and the buckling coefficients of the compressive flange from the solution established by Gardner et al. [10] (i.e. the value of $K_{\mathrm{fb,G}}$) was calculated using the relationship $K_{\mathrm{fb,G}} = K_{\mathrm{wb,G}}/\eta^2$. It can be seen from Figure 12a that the values of the buckling coefficients of the web, determined using Equation (21), were slightly less than those determined using Equation (18) for I-sections with relatively small $t_{\mathrm{f}}/t_{\mathrm{w}}$ and h/b ratios (i.e., $t_{\mathrm{f}}/t_{\mathrm{w}}$ = 1.0 for h/b < 6.7 and $t_{\mathrm{f}}/t_{\mathrm{w}}$ =1.2 for h/b < 5.4), which led to the notable overestimation of $K_{\mathrm{fb,G}}$ shown in Figure 12b. However, the predictions of Equation (21) were always greater than those of Equation (18) for I-sections with relatively large h/b ratios, especially for the cases with large $t_{\mathrm{f}}/t_{\mathrm{w}}$ ratios (see Figure 12a for $t_{\mathrm{f}}/t_{\mathrm{w}}$ = 2.6 and 3.0).

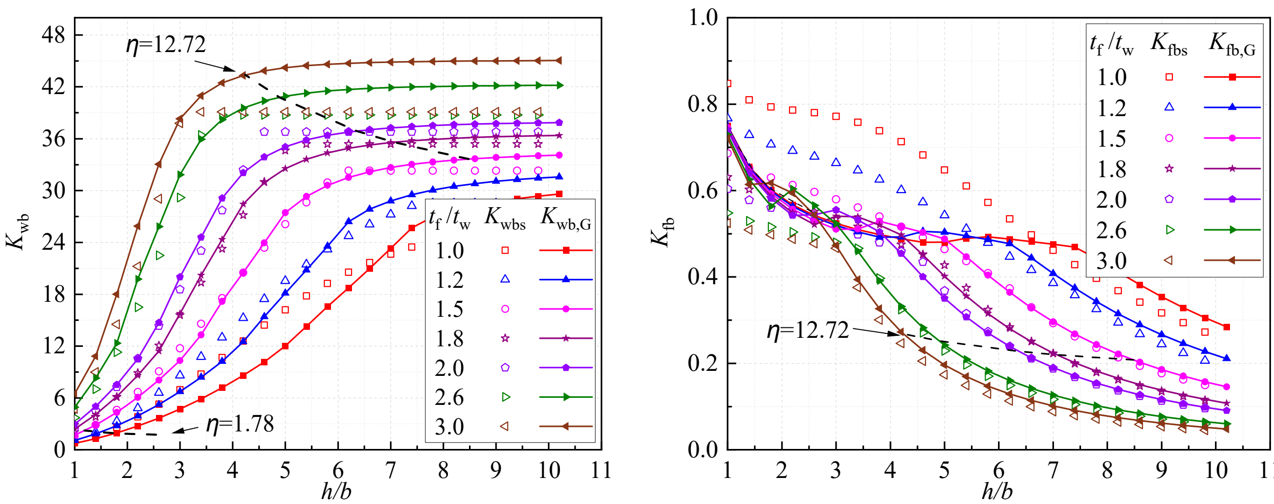

(**a**) K_{wb} (**b**) K_{fb}

Figure 12. Comparisons of K_{wbs} with existing solutions [10].

4. Width-to-Thickness Limit for I-Section Beams

4.1. Method for the Determination of the Width-to-Thickness Limit

The limits of the width-to-thickness ratios for I-section beams could be obtained using Equation (24), similar to reference [15] for I-section columns, as follows:

$$\lambda_{\mathrm{r}} = \left(\frac{b}{t}\right)_{\mathrm{r}} = \alpha_r\sqrt{k\frac{\pi^2}{12(1-\mu^2)}}\sqrt{\frac{E}{f_{\mathrm{y}}}}, \tag{24}$$

where α_r is a constant that considers the effects of residual stress and imperfection, as well as the plasticity-developing requirement of the cross-section, λ (=b/t) is the width-to-thickness ratio of a plate (flange or web), k is the elastic local buckling coefficient of the plate, and E and μ are the elastic modulus and Poisson's ratio of material, respectively. In this study, E = 206,000 N/mm^2 and μ = 0.3 were used (unless otherwise stated).

According to GB50017-2017 [1], the width-to-thickness limits for classes S1, S2, S3, and S4 sections could be taken as 0.5, 0.6, 0.7, and 0.8 times the yield slenderness, respectively (i.e., α_r = 0.5–0.8 for Equation (24)).

The interactions between the width-to-thickness ratios of the compressive flange and the web are shown in Figure 13 for the S1 sections ($\alpha_r = 0.5$). It should be noted that the value of k adopted in Figure 13 was from the FE analyses, and the yield stress f_y was taken as 235 N/mm^2. As shown in Figure 13, the width-to-thickness limits of the compressive flange and the web were no longer constant as long as the flange–web interaction was taken into consideration in the analyses. As shown in Figure 13, all curves of the interaction intersected at a unique point (67, 10), at which point no interaction between the compressive flange and the web existed at the local buckling. For the width-to-thickness ratio of the web (h/t_w, a value smaller than 67), the width-to-thickness limits of b/t_f were greater than 10 due to the rotational restraints of the web. This restraining effect decreased with the increase in the h/t_w ratio, leading to the reduction in the width-to-thickness limit of b/t_f. The compressive flanges turned to provide rotational restraints to the webs when the width-to-thickness ratio of the web, h/t_w, became greater than 67, which resulted in the width-to-thickness ratio of the compressive flange, b/t_f, being smaller than 10. Further, for all the curves shown in Figure 13, the b/t_f limits tended toward 15.72 (corresponding to k = 1.247), with the h/t_w limits approaching zero. It is worth mentioning that k = 1.247 was the upper bound of the buckling coefficient of the compressive flange (i.e., the fixed condition at the flange–web conjunction).

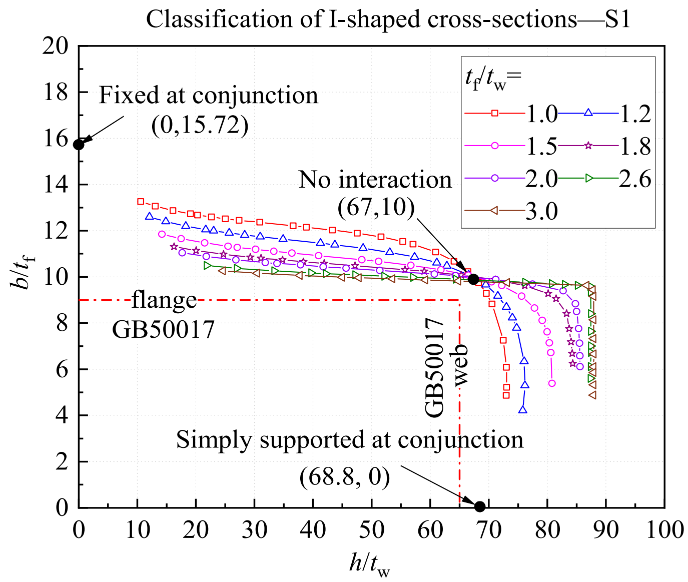

Figure 13. Interactive curves for width-to-thickness ratios of the class S1 sections.

With the decrease in the b/t_f ratio, the width-to-thickness ratios of the web, h/t_w, increased due to the increment in the rotational restraint of the compressive flange, and they reached their respective maximum values at approximately b/t_f = 5–6 in most cases (i.e., t_f/t_w = 1.0–2.0). For the cases with large t_f/t_w ratios (i.e., t_f/t_w = 2.6 and 3.0), the restraints of the compressive flange were strong enough for the web at $b/t_f \leq 9.6$ to achieve the fixed condition at the flange–web conjunction, corresponding to the width-to-thickness limit of the web equal to 88.56 (i.e., k = 39.6). However, the width-to-thickness limit of the web eventually tended toward 68.8 (i.e., k = 29.3) with an extremely small value of b/t_f, where the torsional rigidity of the compressive flange was infinitesimal and the boundary condition of the web at the flange–web conjunction became simply supported.

4.2. Revised Width-to-Thickness Limits

The width-to-thickness limits for class S1 in GB50017 [1] are also shown in Figure 13 using the red dashed-dotted lines. As shown in Figure 13, the constant limits for the compressive flange and web of the I-sections were 9 and 65, respectively. Compared to the FE results of this study, the width-to-thickness limits given in GB50017 [1] were conservative, and therefore, we developed more precise solutions with the flange–web interaction at the local buckling taken into account.

As shown in Figure 14, when the flange–web interaction was considered, the entire $h/t_w - b/t_f$ curves could be divided into the following three zones: the basic zone, the flange-strengthened zone, and the web-strengthened zone. New and simple solutions were then developed, as follows:

$$\left[\frac{h}{t_w}\right] = \left[\frac{h}{t_w}\right]_0 - \frac{\left[\frac{h}{t_w}\right]_0}{\left(\left[\frac{b}{t_f}\right]_f - \left[\frac{b}{t_f}\right]_0\right)^2}\left(\left[\frac{b}{t_f}\right] - \left[\frac{b}{t_f}\right]_0\right)^2 \text{ for } 0 < \frac{h}{t_w} \leq \left[\frac{h}{t_w}\right]_0, \tag{25}$$

$$\left[\frac{h}{t_w}\right] = \left[\frac{h}{t_w}\right]_w - \frac{\left[\frac{h}{t_w}\right]_w - \left[\frac{h}{t_w}\right]_0}{\left(\left[\frac{b}{t_f}\right]_0 - \left[\frac{b}{t_f}\right]_w\right)^2}\left(\left[\frac{b}{t_f}\right] - \left[\frac{b}{t_f}\right]_w\right)^2 \text{ for } \left[\frac{h}{t_w}\right]_0 < \frac{h}{t_w} \leq \left[\frac{h}{t_w}\right]_w, \text{ and} \tag{26}$$

$$\left[\frac{h}{t_w}\right] = \left[\frac{h}{t_w}\right]_w \text{ for } \left[\frac{b}{t_f}\right] \leq \left[\frac{b}{t_f}\right]_w, \tag{27}$$

where $[h/t_w]$ and $[b/t_f]$ are the width-to-thickness limits of the web and the compressive flange, respectively. The subscripts w, 0, and f stand for the three characteristic points W, O, and F (see Figure 14). Of these characteristic points, point O ($[h/t_w]_0$, $[b/t_f]_0$) represents no flange–web interaction, while the points $W([h/t_w]_w, [b/t_f]_w)$ and $F([h/t_w]_f, [b/t_f]_f)$ are the maximum width-to-thickness limits of the web and the compressive flange of each curve, respectively. The values of $[h/t_w]_0$, $[b/t_f]_0$, $[h/t_w]_w$, $[b/t_f]_w$, $[h/t_w]_f$, and $[b/t_f]_f$ for the I-sections of classes S1–S4 are given in Table 2.

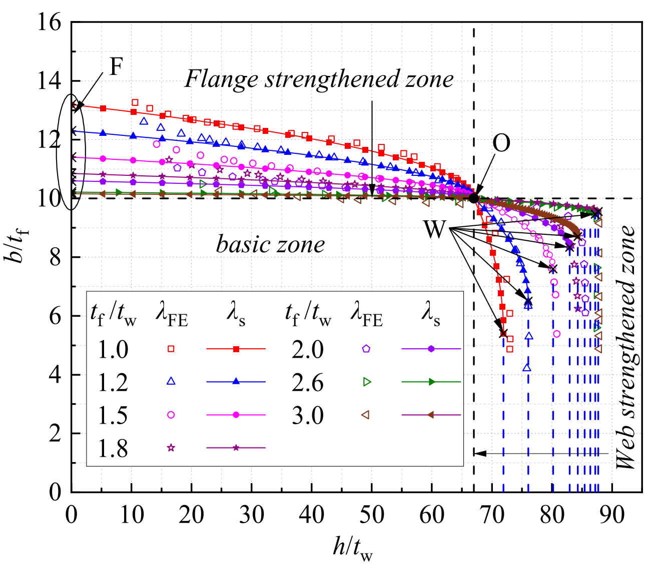

Figure 14. Limits of the width-to-thickness ratios of the class 1 I-sections.

Table 2. The interactive limited values of the width-to-thickness ratios.

	Class			
	S1	**S2**	**S3**	**S4**
$\left[\frac{h}{t_w}\right]_0 / \sqrt{\frac{235}{f_y}}$	67	81	94	107
$\left[\frac{b}{t_f}\right]_0 / \sqrt{\frac{235}{f_y}}$	10	12	14	16
$\left[\frac{b}{t_f}\right]_f / \sqrt{\frac{235}{f_y}}$	$-1.3 + 1.275\zeta + \frac{13.22}{\sqrt{\zeta}}$	$-1.56 + 1.52\zeta + \frac{15.86}{\sqrt{\zeta}}$	$-1.86 + 1.77\zeta + \frac{18.5}{\sqrt{\zeta}}$	$-2.26 + 2\zeta + \frac{21.2}{\sqrt{\zeta}}$
$\left[\frac{h}{t_w}\right]_w / \sqrt{\frac{235}{f_y}}$	$96.7 - \frac{24.8}{\zeta} < 87.7$	$116 - \frac{29.7}{\zeta} < 105.5$	$135.2 - \frac{34.8}{\zeta} < 123.3$	$154.3 - \frac{39.8}{\zeta} < 141$
$\left[\frac{b}{t_f}\right]_w / \sqrt{\frac{235}{f_y}}$	$12 - \frac{6.6}{\zeta} < 9.55$	$14.4 - \frac{8}{\zeta} < 11.46$	$16.8 - \frac{9.4}{\zeta} < 13.37$	$19.2 - \frac{10.8}{\zeta} < 15.28$

Comparisons between the predictions of the solutions illustrated in Equations (25)–(27) (λ_s) and the FE results (λ_{FE}) were made, as shown in Figure 14, and very good agreement could be found between the two. For h/t_w values less than approximately 25, the predictions of Equation (25) for b/t_f were slightly conservative compared to the FE results. As shown in Figure 14, constant values for the width-to-thickness limit of the web, h/t_w, could be calculated using Equation (27) for the regions below point W, which may have led to the overestimation of h/t_w for very small b/t_f values. Fortunately, these extreme values of b/t_f were not within the practical region of the I-beams.

4.3. Evaluation of the Provisions of AISC and EC3

As mentioned in a previous section, the values for α_r are taken as 0.5–0.8 for the S1–S4 class sections in GB50017 [1], while, as listed in Table 3, two parameters (α_r and α_p) are involved in AISC360 [2] and EC3 [3] for the sections of the different classes. In these two design codes, λ_p (using α_p) is used to distinguish the compact and non-compact sections in AISC 360 [2] and the class 2 and class 3 sections in EC3 [3], while λ_r (using α_r) is the criterion for classifying the non-compact and slender sections in AISC 360 [2] and class 3 and class 4 sections in EC3 [3].

Table 3. α_r and α_p given in design codes and used in this paper.

			λ_p Design Codes	α_p Design Codes	α_p In this Section	λ_r Design Codes	α_r Design Codes	α_r In this Section
AISC	Rolled I-shaped sections	Flange	$0.38\sqrt{E/f_y}$	0.46 [a]	0.46	$1.0\sqrt{E/f_y}$	1.0 [a]	1.0
		Web	$3.76\sqrt{E/f_y}$	0.58 [a]	0.58	$5.7\sqrt{E/f_y}$	1.0 [a]	1.0
	Built-up I-shaped sections	Flange	$0.38\sqrt{E/f_y}$	0.46 [a]	0.46	$0.95\sqrt{k_c E/(0.7f_y)}$ $0.35 \le k_c = \frac{4}{\sqrt{h/t_w}} \le 0.76$	1.19 [a]	1.19
		Web	$3.76\sqrt{E/f_y}$	0.58 [a]	0.58	$5.7\sqrt{E/f_y}$	1.0 [a]	1.0
EC3		Flange	$10\sqrt{235/f_y}$	0.54 [b]	0.54	$14\sqrt{235/f_y}$	0.751 [b] 0.748 [c]	0.751
		Web	$83\sqrt{235/f_y}$	0.60 [b]	0.60	$124\sqrt{235/f_y}$	0.893 [b] 0.874 [c]	0.893

[a], given by reference [9]; [b], back-calculated by Equation (24) using λ_p or λ_r from EC3 [3] and k of a simply supported plate, respectively; [c], given by EC3 parts 1–5 [24].

The width-to-thickness limits given in AISC360 [2] and EC3 [3] were compared with those calculated using the FE results, as shown in Figure 15, where the interaction curves of the FE results were obtained using the buckling coefficients calculated from the FE results associated with the same α_r(or α_p) as the design codes (see Table 3). Therefore, with this treatment, the differences in the width-to-thickness limits between the FE results and the design codes were only due to the different buckling coefficients, as the limits of the width-to-thickness ratio using Equation (24) were dependent on both k and α_r (or α_p). It can be seen from Figure 15a that the width-to-thickness limits given in AISC [2] for the non-compact sections were greater than those obtained using the FE results for most of the rolled I-sections. However, the predictions of AISC [2] for the built-up sections were nearly at the lower bound of the results of the FE analyses, except for slight overestimations for the web of the I-sections with t_f/t_w values less than 1.8 (Figure 15b). This was because, as mentioned in AISC [2], the flange–web interactions were partially considered for the built-up sections. As shown in Figure 15c, the width-to-thickness limits given in AISC [2] for the compact sections were the same for both the rolled and built-up sections, which were greater than the results from the FE analyses for both the compressive flange and the web, in most cases (Figure 15c). It should be noted that the width-to-thickness limits of AISC [2] were determined based on the condition that four times the yield strain could be achieved in the compressive flange prior to the local buckling occurring (i.e., $\psi = 4$) or the rotation capacity R could exceed 3.0 [25,26]. The width-to-thickness limits in EC3 [3] for the class 2 and class 3 I-sections were smaller than those in the FE results (Figure 15d,e).

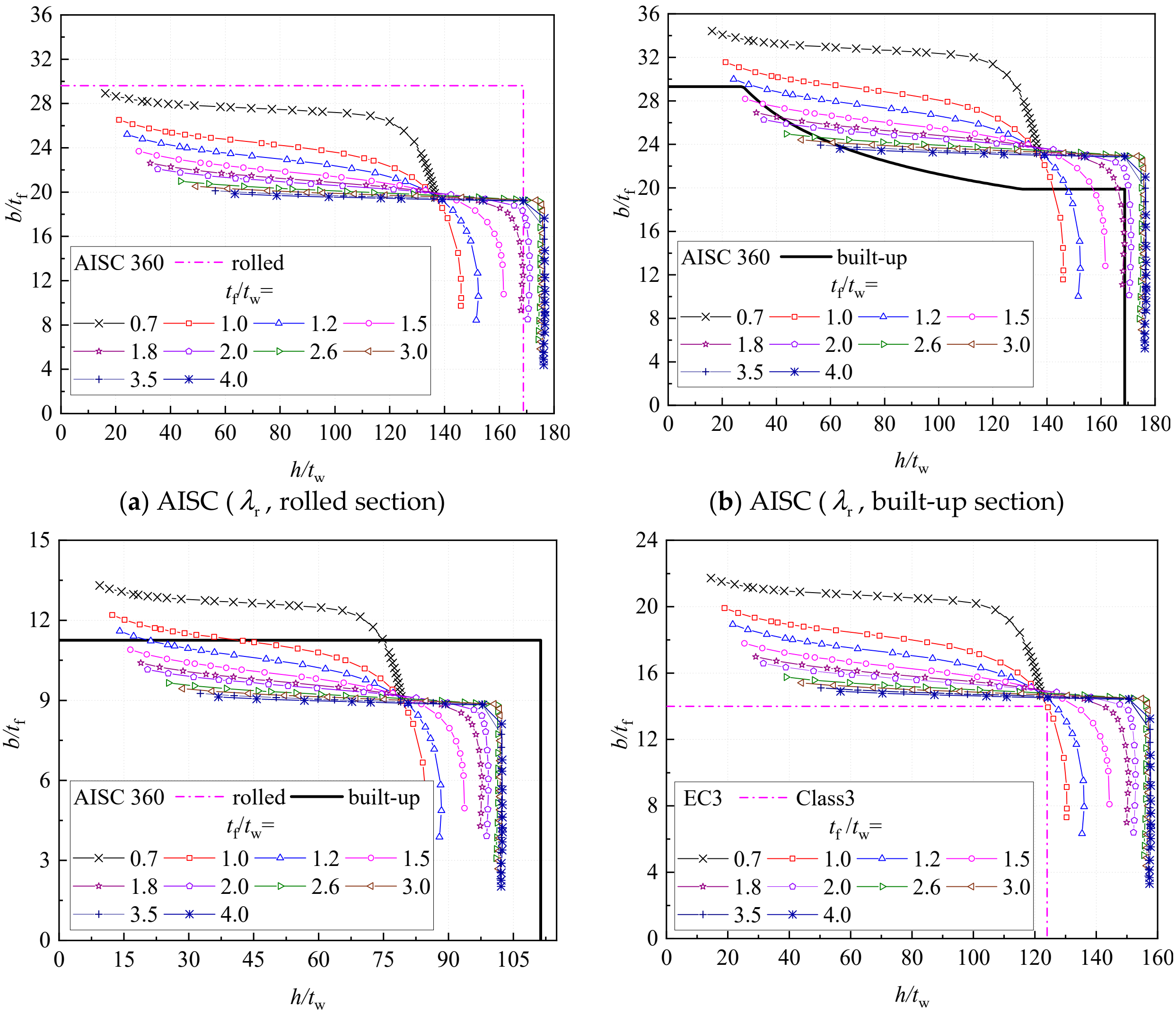

(**a**) AISC (λ_r , rolled section) (**b**) AISC (λ_r , built-up section)

(**c**) AISC (λ_p) (**d**) EC3 (Class 3)

Figure 15. *Cont.*

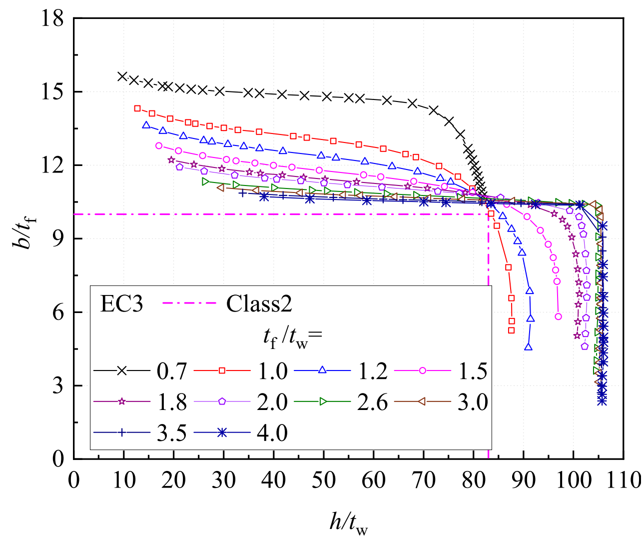

(**e**) EC3(Class 2)

Figure 15. Comparisons of the width-to-thickness ratio limits with the specifications.

4.4. Comparison with Solutions in Existing Studies

A numerical program was developed by Ragheb et al. [13] to determine the inelastic local buckling of I-section members. By considering the initial deformation and residual stresses, the solutions for the width-to-thickness limits by taking the flange–web interactions into consideration were proposed. The limits of b/t_f for the compressive flange buckling can be calculated as follows:

$$\lambda_p = 0.61\sqrt{\frac{E}{f_y}} / \left[\left(\frac{B}{h}\right)^{0.15} \left(\frac{h}{t_w}\right)^{0.18} \right] \text{ and} \tag{28}$$

$$\lambda_r = \sqrt{\frac{E}{f_y}} / \left[\left(\frac{B}{h}\right)^{0.20} \left(\frac{h}{t_w}\right)^{0.10} \right], \tag{29}$$

and the limits of h/t_w for the web buckling can be calculated as follows:

$$\lambda_p = 2.75\sqrt{\frac{E}{f_y}} \cdot \left(\frac{B}{h}\right)^{0.10} \text{ and} \tag{30}$$

$$\lambda_r = 5.8\sqrt{\frac{E}{f_y}} \cdot \left(\frac{B}{h}\right)^{0.035}, \tag{31}$$

where the flange width $B = 2b$ and the limits λ_p and λ_r correspond to the rotation index ψ of 4 and 1, respectively. ψ is defined as the rotation of the beam at the local buckling over the rotation of the beam at yield. As shown in Figure 16a,b, the predictions of Equations (28)–(31) were compared with those from the solutions of the present study (Equations (25)–(27)) for I-sections with h/b values equal to 2.0. The values of the elastic modulus E and the yield stress f_y adopted herein were 200,000 N/mm^2 and 250 N/mm^2, respectively. It can be seen from Figure 16a,b that the width-to-thickness limits proposed by Ragheb [13] were greater than those obtained using the solutions in this study for non-compact sections (equivalent to class 3 or S4), but they were conservative for compact sections (equivalent to class 2 or S2). As shown in Figure 16a,b, the width-to-thickness limits of the compressive flange decreased with increases in the h/t_w ratio, which was the case for the predictions of both solutions. It should be noted that the variations in b/t_f and h/t_w, as shown in Figure 16a,b, were achieved by varying the values of t_f/t_w, as the aspect ratio h/b was fixed at 2.0.

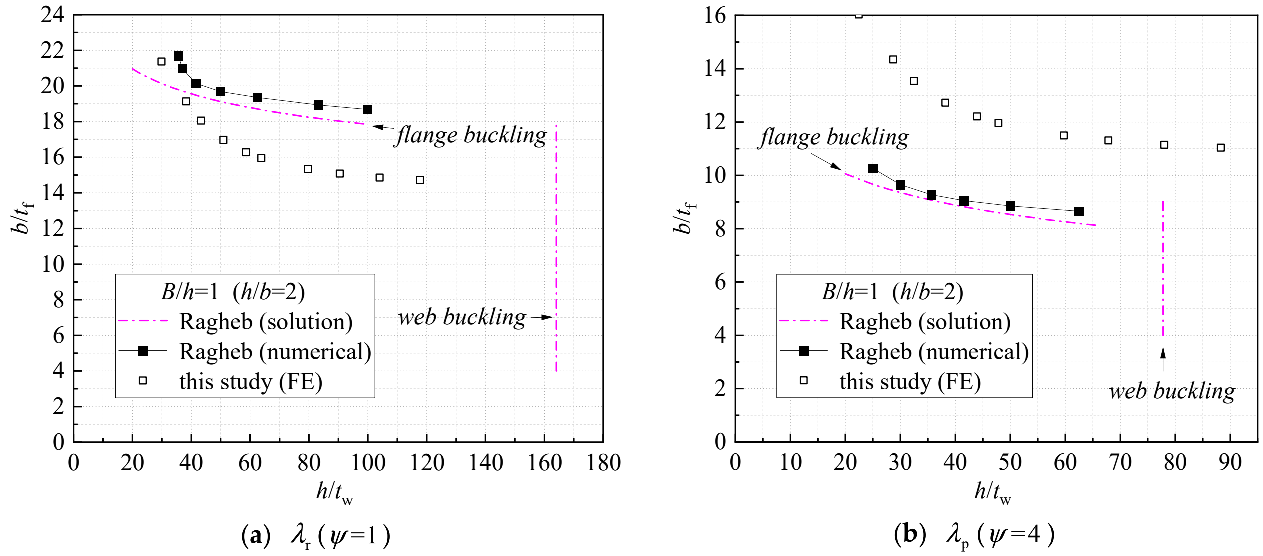

Figure 16. Comparison of the interactive curves for the width-to-thickness limits.

More comparisons between these two solutions were made, as shown in Figure 17a,b. In order to obtain the relationship between b/t_f and h/t_w, Equations (28)–(31) were rewritten as follows: for the compressive flange buckling of compact sections,

$$\left(\frac{b}{t_f}\right)^{1.15} = \left[0.55\sqrt{\frac{E}{f_y}}/\left(\frac{t_f}{t_w}\right)^{0.15}\right]\left(\frac{h}{t_w}\right)^{-0.03}; \tag{32}$$

for the compressive flange buckling of non-compact sections,

$$\left(\frac{b}{t_f}\right)^{1.20} = \left[0.87\sqrt{\frac{E}{f_y}}/\left(\frac{t_f}{t_w}\right)^{0.20}\right]\left(\frac{h}{t_w}\right)^{0.1}; \tag{33}$$

for the web buckling of compact sections,

$$\left(\frac{h}{t_w}\right)^{1.1} = \left[2.95\sqrt{\frac{E}{f_y}}\left(\frac{t_f}{t_w}\right)^{0.10}\right]\left(\frac{b}{t_f}\right)^{0.10}; \text{ and} \tag{34}$$

for the web buckling of non-compact sections,

$$\left(\frac{h}{t_w}\right)^{1.035} = \left[5.94\sqrt{\frac{E}{f_y}}\left(\frac{t_f}{t_w}\right)^{0.035}\right]\left(\frac{b}{t_f}\right)^{0.035}. \tag{35}$$

Using Equations (32)–(35), the relationships between b/t_f and h/t_w could be identified with different t_f/t_w ratios (λ_R in Figure 17a,b). All the results presented in Figure 17 were obtained using E = 200,000 N/mm^2 and f_y = 250 N/mm^2. As shown in Figure 17a, for the non-compact I-sections (i.e., class S4), the variations in the predictions of Equation (33) and Equations (25)–(27) (λ_s) for certain t_f/t_w values with increases in h/t_w were different for the I-sections that failed during the compressive flange-dominated local buckling. Moreover, it was also shown that the width-to-thickness limits from Equation (33) were slightly greater than those obtained from Equations (25)–(27) for the I-sections that failed during the web-dominated local buckling. For the compact sections (i.e., class S2), the width-to-thickness limits from Equations (32) and (34) were smaller than those obtained from Equations (25)–(27) for both the compressive flange and the web. It should be noted that the method for the determination of the width-to-thickness limits of the I-sections in the study by Ragheb [13] was based on an inelastic numerical analysis, which was different from that used in this study.

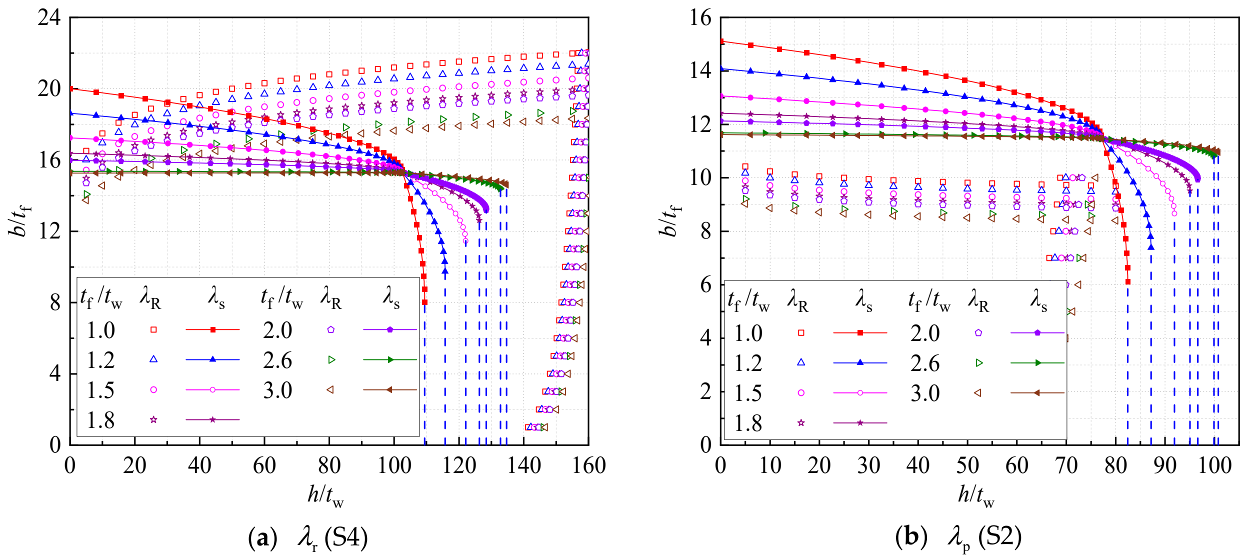

Figure 17. Comparison of the interactive curves for the limits of the width-to-thickness ratios.

5. Conclusions

By taking the flange–web interactions into account, the elastic local buckling and width-to-thickness limits of I-section beams were investigated in this study. Simple solutions for the elastic local buckling coefficients for I-sections under pure bending incorporating flange–web interactions were developed through the energy method and refined based on the FE results. The predictions of the presented solutions were in very good agreement with the FE results and much better than those obtained using existing solutions. Using the simple solutions for the buckling coefficients, the limits for the width-to-thickness ratios of I-section beams were also proposed. The proposed limits were then compared with those from the FE analyses and design codes, which also indicated the superiority of the proposed solutions.

Author Contributions: Investigation, L.Z., Q.Z. (Qianjing Zhang), G.T. and Q.Z. (Qunhong Zhu); Writing—original draft, Q.Z. (Qianjing Zhang); Writing—review & editing, Q.Z. (Qunhong Zhu); Supervision, G.T. All authors have read and agreed to the published version of the manuscript.

Funding: This work is partially supported by the "2021 Annual Vocational College Industry-Education Cooperation Collaborative Education Project of China". The support is greatly appreciated.

Data Availability Statement: The data presented in this study are available on request from the corresponding author. The data are not publicly available due to privacy.

Conflicts of Interest: The authors declare no conflict of interest.

References

1. *GB50017-2017*; Standard for Design of Steel Structures. China Architecture & Building Press: Beijing, China, 2017.
2. *ANSI/AISC 360-16*; Specification for Structural Steel Buildings. American Institute of Steel Construction: Chicago, IL, USA, 2016.
3. *EN 1993-1-1*; Eurocode 3: Design of Steel Structures—Part 1-1: General Rules and Rules for Buildings. European Committee for Standardization: Brussels, Belgium, 2005.
4. Bleich, F. *Buckling Strength of Metal Structures*; Mc Graw-Hill Book Company, Inc.: New York, NY, USA, 1952.
5. Timoshenko, S.P.; Gere, J.M. *Theory of Elastic Stability*, 2nd ed.; McGraw-Hill: New York, NY, USA, 1961.
6. Kroll, W.D.; Fisher, G.P.; Heimerl, G.J. *Charts for Calculation of the Critical Stress for Local Instabilty of Columns with I-, Z-, Channel, and Rectangular-Tube Section*; NACA: Washington, DC, USA, 1943.
7. Lundquist, E.E.; Stowell, E.Z. *Critical Compressive Stress for Flat Rectangualr Plates Supported along all Edges and Elastically Restrained against Rotation along the Unloaded Edges*; NACA: Washington, DC, USA, 1942.
8. Peng, G. The Research on Local Buckling of Thin-Walled Section. Master's Thesis, Zhejiang University, Hangzhou, China, 2012.

9. Seif, M.; Schafer, B.W. Local buckling of structural steel shapes. *J. Constr. Steel Res.* **2010**, *66*, 1232–1247. [CrossRef]
10. Gardner, L.; Fieber, A.; Macorini, L. Formulae for Calculating Elastic Local Buckling Stresses of Full Structural Cross-sections. *Structures* **2019**, *17*, 2–20. [CrossRef]
11. Jin, Y.; Tong, G. Elastic Buckling of Web Restrained by Flanges in I-section members. *J. Zhejiang Univ. Eng. Sci.* **2009**, *43*, 1883–1891.
12. Vieira, L.; Gonçalves, R.; Camotim, D. On the local buckling of RHS members under axial force and biaxial bending. *Thin Wall Struct.* **2018**, *129*, 10–19. [CrossRef]
13. Ragheb, W.F. Local buckling of welded steel I-beams considering flange–web interaction. *Thin Wall Struct.* **2015**, *97*, 241–249. [CrossRef]
14. Johnson, D.L. An Investigation into the Interaction of Flanges and Webs in Wide-Flange Shapes. In Proceedings of the Annual Technical Session and Meeting, Cleveland, OH, USA, 16–17 April 1985; pp. 395–405.
15. Zhang, Q.; Zhang, L.; Zhang, Y.; Liu, Y.; Zhou, J. Elastic Local Buckling of I-Sections under Axial Compression Incorporating Web–Flange Interaction. *Buildings* **2023**, *13*, 1912. [CrossRef]
16. Wu, R.; Wang, L.; Tong, J.; Tong, G.; Gao, W. Elastic buckling formulas of multi-stiffened corrugated steel plate shear walls. *Eng. Struct.* **2024**, *300*, 117218. [CrossRef]
17. Bulson, P.S. *The Stability of Flat Plates*; Chatto and Windus: London, UK, 1970.
18. Szychowski, A. Computation of thin-walled cross-section resistance to local buckling with the use of the Critical Plate Method. *Arch. Civ. Eng.* **2016**, *62*, 229–264. [CrossRef]
19. Szychowski, A.; Brzezińska, K. Local buckling and resistance of continuous steel beams with thin-walled I-shaped cross-sections. *Appl. Sci.* **2020**, *10*, 4461. [CrossRef]
20. Chen, S.; Liu, J.; Chan, T. Local buckling behaviour of high strength steel and hybrid I-sections under axial compression: Numerical modelling and design. *Thin Wall Struct.* **2023**, *191*, 111079. [CrossRef]
21. ANSYS. *ANSYS Release 17.0 Documentation*; ANSYS: Canonsburg, PA, USA, 2015.
22. Ragheb, W.F. Local buckling analysis of pultruded FRP structural shapes subjected to eccentric compression. *Thin Wall. Struct.* **2010**, *48*, 709–717. [CrossRef]
23. Tong, G. *Out-of-Plane Stability of Steel Structures (Revised Version)*; China Architecture & Building Press: Beijing, China, 2012.
24. *EN 1993-1-5*; Eurocode 3: Design of Steel Structures—Part 1-5: Plated Structrual Elements. European Committee for Standardization: Brussels, Belgium, 2006.
25. Lukey, A.F.; Adams, P.F. Rotation capacity of beams under moment gradient. *J. Struct. Div.* **1969**, *95*, 1173–1188. [CrossRef]
26. Yura, J.A.; Galambos, T.V.; Ravindra, M.K. The bending resistance of steel beams. *J. Struct. Div.* **1978**, *104*, 1355–1370. [CrossRef]